NeuroImage: Clinical 31 (2021) 102692

Contents lists available at ScienceDirect

NeuroImage: Clinical

journal homepage: www.elsevier.com/locate/ynicl

Longitudinal [^{18}F]FDG and [^{13}N]NH_3 PET/CT imaging of brain and spinal cord in a canine hemisection spinal cord injury model

Lijian Zhang [a,b,1], Francisco R. López-Picón [c,d,1], Yingqin Jia [e], Yao Chen [a], Juan Li [e], Chunlei Han [f], Xiaoqing Zhuang [e,*], Hechun Xia [a,*]

[a] Department of Neurosurgery, General Hospital of Ningxia Medical University, Yinchuan, Ningxia, China
[b] Department of Neurosurgery, Affiliated Hospital of Hebei University, Baoding, Hebei, China
[c] Preclinical Imaging Laboratory, Turku PET Centre, University of Turku, Turku, Finland
[d] MediCity Research Laboratory, University of Turku, Turku, Finland
[e] Department of Nuclear Medicine, General Hospital of Ningxia Medical University, Yinchuan, Ningxia, China
[f] Clinical Imaging Laboratory, Turku PET Centre, University of Turku and Turku University Hospital, Turku, Finland

ARTICLE INFO

Keywords:
Spinal cord injury
Canine
Glutamine synthetase
[^{13}N]NH_3
Blood spinal cord barrier (BSCB)
Longitudinal PET/CT imaging

ABSTRACT

To further understand the neurological changes induced by spinal cord injury (SCI) in its acute and subacute stages, we evaluated longitudinal changes in glucose and glutamate metabolism in the spinal cord and brain regions of a canine hemisection SCI model. [^{18}F]FDG and [^{13}N]NH_3 positron-emission tomography (PET) with computed tomography (CT) was performed before SCI and at 1, 3, 7, 14, and 21 days after SCI. Spinal cord [^{18}F]FDG uptake increased and peaked at 3 days post SCI. Similar changes were observed in the brain regions but were not statistically significant. Compared to the acute phase of SCI, [^{13}N]NH_3 uptake increased in the subacute stage and peaked at 7 days post SCI in all analyzed brain regions. But in spinal cord, no [^{13}N]NH_3 uptake was detected before SCI when the blood-spinal cord barrier (BSCB) was intact, then gradually increased when the BSCB was damaged after SCI. [^{13}N]NH_3 uptake was significantly correlated with plasma levels of the BSCB disruption marker, monocyte chemoattractant protein-1 (MCP-1). Overall, we showed that SCI induced *in vivo* changes in glucose uptake in both the spinal cord and the examined brain regions, and changes in glutamine synthetase activity in the latter. Moreover, our results suggest that [^{13}N]NH_3 PET may serve as a potential method for assessing BSCB permeability *in vivo*.

1. Introduction

Spinal cord injury (SCI) is a devastating neurological condition, owing to the cord's limited capacity for repair. SCI damages efferent and afferent neural pathways and inevitably lead to changes in brain structure and function (Hains et al., 2005; Wrigley et al., 2009; Freund et al., 2011; Wu et al., 2014a). Neuroplasticity after SCI, including metabolic and structural changes, have been extensively discussed and reviewed (Athanasiou et al., 2017; Solstrand Dahlberg et al., 2018; Mohammed et al., 2018), but most studies have focused on the chronic phase of SCI. Due to the complexity of the connection between brain and spinal cord, there are still many unknowns regarding alterations in the spinal cord and brain during the acute and subacute phases of SCI.

Glucose is the main energy source for the mammalian brain. Glucose metabolism provides both energy and precursors for the biosynthesis of neurotransmitters (Mergenthaler et al., 2013). The PET tracer 2-deoxy-2-[^{18}F]fluoroglucose ([^{18}F]FDG) is an glucose analog used to investigate glucose metabolism *in vivo*. It has been used to investigate sensorimotor network reorganization in the chronic stage of SCI (Roelcke et al., 1997) and the integrated synaptic activity of SCI patients with chronic neuropathic pain after SCI (Yoon et al., 2013, 2014).

Glutamate is an important neurotransmitter and upon injury, neurons release excess glutamate causing neurotoxicity after trauma (Rothman and Olney, 1986; Choi and Rothman, 1990). Catalyzed by glutamine synthetase (GS), glutamate and ammonium react to yield glutamine (Cooper et al., 1979; Cooper and Plum, 1987), which is nontoxic and a substrate in protein and purine synthesis (Zalkin and Smith, 1998). The oxidation of glutamine through the tricarboxylic acid

* Corresponding authors.
E-mail addresses: zhuangxq@nyfy.com.cn (X. Zhuang), xhechun@nyfy.com.cn (H. Xia).
[1] Both authors contributed equally to this work.

https://doi.org/10.1016/j.nicl.2021.102692
Received 16 January 2021; Received in revised form 21 April 2021; Accepted 1 May 2021
Available online 4 May 2021

cycle is also a potential source of energy for the brain (Tildon and Roeder, 1984). Thus, GS plays an important role in regulating glutamate and glutamine levels in the central nervous system (Benton et al., 2000). [^{13}N]Ammonia ([^{13}N]NH_3) is a PET tracer used for imaging and measuring myocardial and cerebral blood flows in the clinic. Late-phase [^{13}N]NH_3 PET imaging shows the distribution of [^{13}N]glutamine in brain, and changes in cerebral [^{13}N]NH_3 accumulation reflect changes in GS activity (Momosaki et al., 2015).

A detailed analysis of glucose uptake and GS activity during the acute and subacute phases of SCI in the spinal cord and specific brain regions has not yet been conducted. In this longitudinal study, we aimed to investigate changes in glucose uptake and GS activity in certain brain regions and the spinal cord from baseline before injury to the subacute stage of SCI. We used a canine model of SCI, taking advantage of the heterogeneity of dog genetic backgrounds and the histopathological similarities between dogs and humans (Bock et al., 2013; Moore et al., 2017).

2. Materials and methods

2.1. Animals

We used eight male beagle dogs (1 to 2 years old, 13–17 kg) from the Experimental Animal Centre of Ningxia Medial University. Dogs were divided into two groups: a control group (n = 3) for immunohistochemical study and an SCI group (n = 5) for the longitudinal PET/CT study. All dogs were individually housed under consistent temperature (21–25 °C) and humidity (30–40%) and standard 12-h light/dark conditions. The dogs were fed standard dog chow twice daily with water available *ad libitum*. The protocols used in this study were approved by the Animal Ethics Board of the General Hospital of Ningxia Medical University (2017-073). The ethical standards were in compliance with the Helsinki Declaration and the national guidelines for the care and use of animals.

2.2. Establishment of a hemisection SCI model

All five dogs in the SCI group were given tramadol hydrochloride (CSPC Pharmaceutical Co., Shijiazhuang, China; 2.5 mg/kg, intramuscularly) 30 min before the operation, and for 3 days after surgery for postoperative analgesia. Dogs were anesthetized with dexmedetomidine (Dexdomitor; Orion Corporation, Espoo, Finland; 10 μg/kg, intramuscularly), and spontaneous ventilation was maintained with 2.5–3.0% isoflurane in oxygen. To maintain body temperature, the dogs were placed on a heating pad. After preparing the skin, a laminectomy was performed at the tenth thoracic segment (T10), followed by a unilateral left-side hemisection at the T10 level, which was performed with microscissors (Zhang et al., 2020). After the operation, manual bladder expression was performed at least three times per day until voluntary urination was established. The general condition and neurological status of the dogs were monitored twice daily during the study period and there were no complications (Ryu et al., 2009). The study design is illustrated in Fig. 1A.

2.3. Image protocol

PET/CT studies were performed before and 1, 3, 7, 14, 21 days after SCI. [^{13}N]NH_3 PET/CT and [^{18}F]FDG PET/CT imaging were performed on the same study day (Fig. 1B). Before PET/CT imaging, dogs were fasted overnight. Anesthesia was induced with an intramuscular injection of dexmedetomidine (10 μg/kg, intramuscularly), and maintained with 2.5–3.0% isoflurane in oxygen. Next, the dogs were placed on the bed of the PET/CT scanner (Discovery VCT, 64-MSCT, GE HealthCare, USA). After intravenous injection of 425 ± 46 MBq [^{13}N]NH_3 into the cephalic vein, a CT scan was performed (non-enhanced, low-dose, 120 kV, 40–100 mA, slice thickness: 3.75 mm) for attenuation correction and positioning. A static PET scan was then acquired in 3D mode, 5–30 min after [^{13}N]NH_3 injection. After [^{13}N]NH_3 PET/CT scanning, 264 ± 8 MBq [^{18}F]FDG was intravenously injected through the cephalic vein. Static PET imaging was acquired at 60–85 min after [^{18}F]FDG injection. Transaxial emission images with a thickness of 3.27 mm were reconstructed in a 128 × 128 matrix with an iterative reconstruction algorithm, and the images were corrected for attenuation.

MRI studies were performed on a 3 T GE Signa PET/MRI (Signa, GE HealthCare, USA). The T1-weighted images were acquired in a 3D acquisition type with following parameters: dimensions = 512 × 512 × 96, voxel size = 0.35 × 0.35 × 2 mm^3, repetition time (TR) = 7.1 ms, echo time (TE) = 2.7 ms, inversion time = 450 ms, number of averages = 2, slice thickness = 2 mm, spacing between slices = 2 mm, images in acquisition = 96, flip angle = 15°, acquisition matrix = 256 × 224.

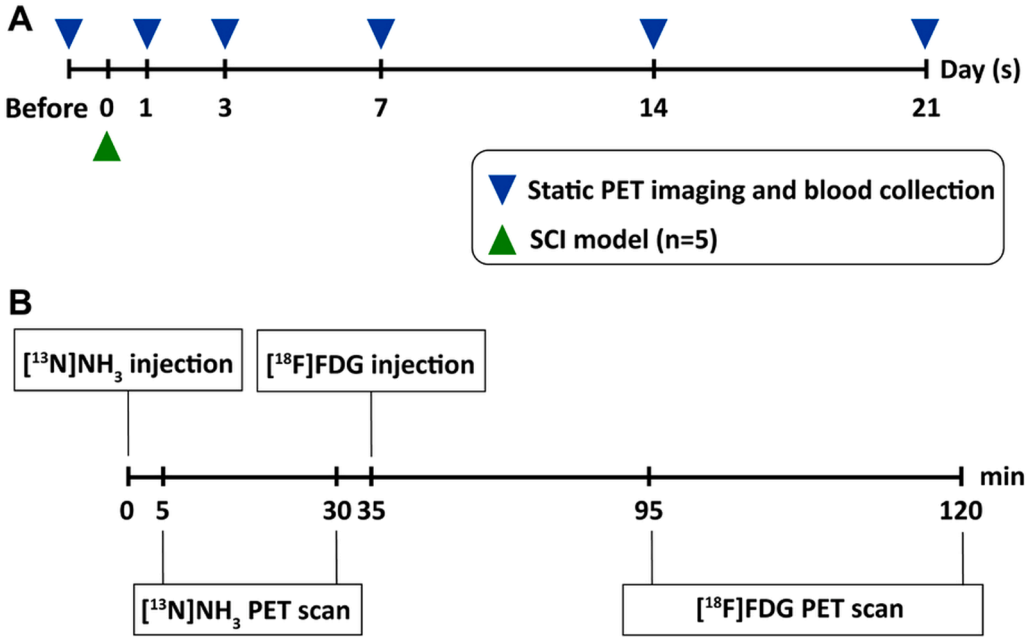

Fig. 1. The design of the study. (A) Schematic diagram of the study protocol. (B) Diagram of the [^{18}F]FDG and [^{13}N]NH_3 PET/CT scanning.

2.4. Image analysis

For brain regions, the 3D volumes-of-interest (VOIs) of left and right cortex, left and right white matter, left and right caudate-putamen, and cerebellum were manually drawn using T1 MRI images by Inveon Research Workplace (IRW) Image Analysis software v. 4.1 (Siemens Medical Solutions) and saved as an atlas template (Fig. 2). Then the MRI and PET images were co-registered by automatic registration using the IRW and the previous generated ROIs were placed over the MRI images (Fig. 3). The mean standardized uptake value (SUV) of each brain region was automatically measured by the software. The SUV ratio (SUV_r) was calculated as the ratio of the SUV value at each time point to the SUV value before injury.

PET images of spinal cord were processed at the Turku PET Centre using Carimas v.2.10 software (Turku PET Centre; http://www.turkupetcentre.fi/carimas). 3D VOIs of [^{13}N]NH_3 were identified in the spinal cord at the T9-T10 region, and VOIs of [^{18}F]FDG were identified at the T9-T11 region. The SUV (mean standardized uptake value) was measured on fused PET and CT image. Reference VOI was identified in the spinal cord at the T4-T5 region. $SUV_{reference}$ value was the mean standardized uptake value in the reference region. SUV_r was calculated as the ratio of SUV to $SUV_{reference}$.

2.5. Measurement of plasma MCP-1 levels

Arterial blood samples were collected with a 24-G intravenous catheter connected to a lithium heparin tube (both from Becton Dickinson, Oxford, UK). Samples were collected before SCI and at 1, 3, 7, 14, and 21 days after SCI. Samples were centrifuged immediately after collection (2000 × g, 10 min, 4 °C), and the plasma was stored at − 80 °C until assayed. We measured plasma MCP-1 levels with a solid-phase, sandwich, enzyme-linked immunosorbent assay (ELISA) kit (RayBiotech, Norcross, GA, United States). Assays were performed according to the manufacturer's instructions.

2.6. Immunohistochemical assay

All dogs were euthanized with potassium chloride (Sigma-Aldrich, Gillingham, UK, P3911-25G, 75 mg/kg, intravenously) in deep anesthesia (2.5–3.0% isoflurane in oxygen). Immediately after euthanasia a complete postmortem examination was performed. All dogs were perfused with saline. Spinal cord sections from the tenth thoracic segment were dissected and fixed in 10% formalin and embedded in paraffin using routine procedures. Serial transverse sections (5 μm) were cut from paraffin blocks. To investigate the penetrability of the blood-spinal cord barrier, immunohistochemistry assays were performed. Sections were incubated with an anti-zonula occluden 1 (ZO-1) polyclonal antibody (1:200, Invitrogen, 40-2200, Carlsbad, CA, USA). Biotinylated anti-rabbit secondary antibodies (1:5000, Invitrogen, 31460, Carlsbad, CA, USA) were added and incubated at 37 °C for 2 h. Finally, immunohistochemistry images were obtained using a light microscope (Leica DM4000 M, Germany). Average values of integrated optical density (IOD) were obtained from three random fields per slide using Image-Pro Plus software (Media Cybernetics, Rockville, MD, USA).

2.7. Statistical analyses

The results are expressed as the mean ± SD, and all statistical analyses were performed at the Turku PET Centre with GraphPad Prism Software 7.0 (GraphPad Software, La Jolla, CA, USA). A one-way ANOVA with Tukey's post hoc test was used for multiple comparisons. Correlation analyses were performed with Pearson's product moment (r) correlation. Differences were considered statistically significant at $p < 0.05$.

3. Results

3.1. Longitudinal [^{13}N]NH_3 and [^{18}F]FDG PET imaging in brain

The [^{13}N]NH_3 uptake in all analyzed brain regions had the same trend (Fig. 4). The uptake ratios decreased slightly at 1 day post SCI,

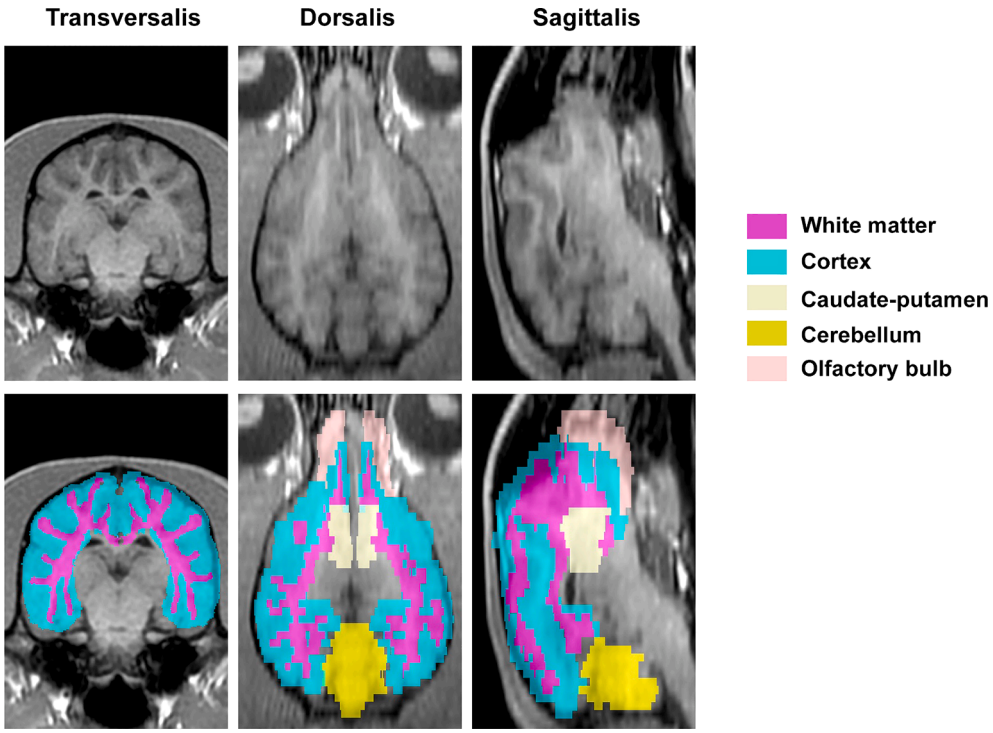

Fig. 2. Co-registered PET/CT images showing atlas-based analysis using the Inveon Research Work-place. Image showing 6 regions from the canine brain atlas (VOI) registered to the MRI data.

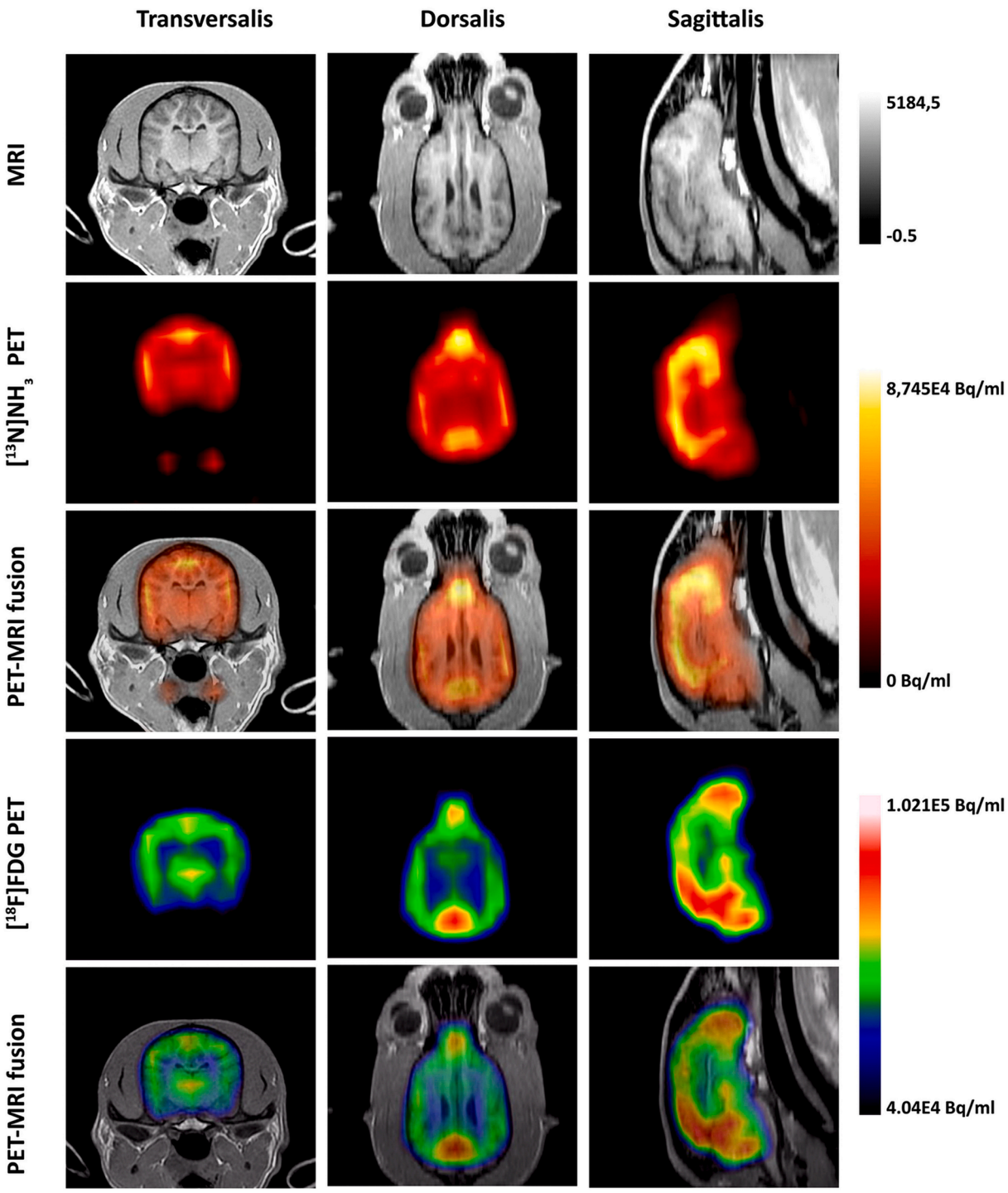

Fig. 3. Representative [^{18}F]FDG and [^{13}N]NH_3 co-registered PET/MRI images acquired in normal beagle dogs.

although they did not reach a significantly different level compared with that before injury ($p > 0.05$, $n = 5$). The [^{13}N]NH_3 uptake ratios then gradually increased to a peak at 7 days post SCI. Significantly higher [^{13}N]NH_3 uptake ratios were evident at 7 days post SCI than at 1 day in the right cortex (0.80 ± 0.23 vs 1.59 ± 0.26, $p = 0.0088$, $n = 5$), left cortex (0.80 ± 0.22 vs 1.60 ± 0.42, $p = 0.0052$, $n = 5$), right white matter (0.70 ± 0.24 vs 1.66 ± 0.42, $p = 0.026$, $n = 5$), left white matter (0.78 ± 0.20 vs 1.60 ± 0.41, $p = 0.005$, $n = 5$), right caudate-putamen (0.78 ± 0.21 vs 1.58 ± 0.41, $p = 0.0082$, $n = 5$), left caudate-putamen (0.78 ± 0.203 vs 1.59 ± 0.42, $p = 0.0078$, $n = 5$), and cerebellum (0.80 ± 0.25 vs 1.69 ± 0.52, $p = 0.0068$, $n = 5$). However, there was no significant difference between the [^{13}N]NH_3 uptake ratios at 7 days and before injury ($p > 0.05$, $n = 5$). Thereafter, the [^{13}N]NH_3 uptake ratios decreased in all brain regions. We measured the ratios of [^{13}N]NH_3 uptake between the right and left cerebral hemisphere regions, and there was no significant intergroup difference ($p > 0.05$, $n = 5$) (Supplementary Fig. 1). The [^{13}N]NH_3 uptake ratios between the analyzed regions and the whole brain were calculated and there was no significant intergroup difference ($p > 0.05$, $n = 5$) (Supplementary Fig. 2).

The [^{18}F]FDG accumulation in brain regions showed little change after SCI (Fig. 5). In all brain regions, [^{18}F]FDG uptake decreased slightly but nonsignificantly at 1 day post-SCI. Then, similar to the [^{18}F]

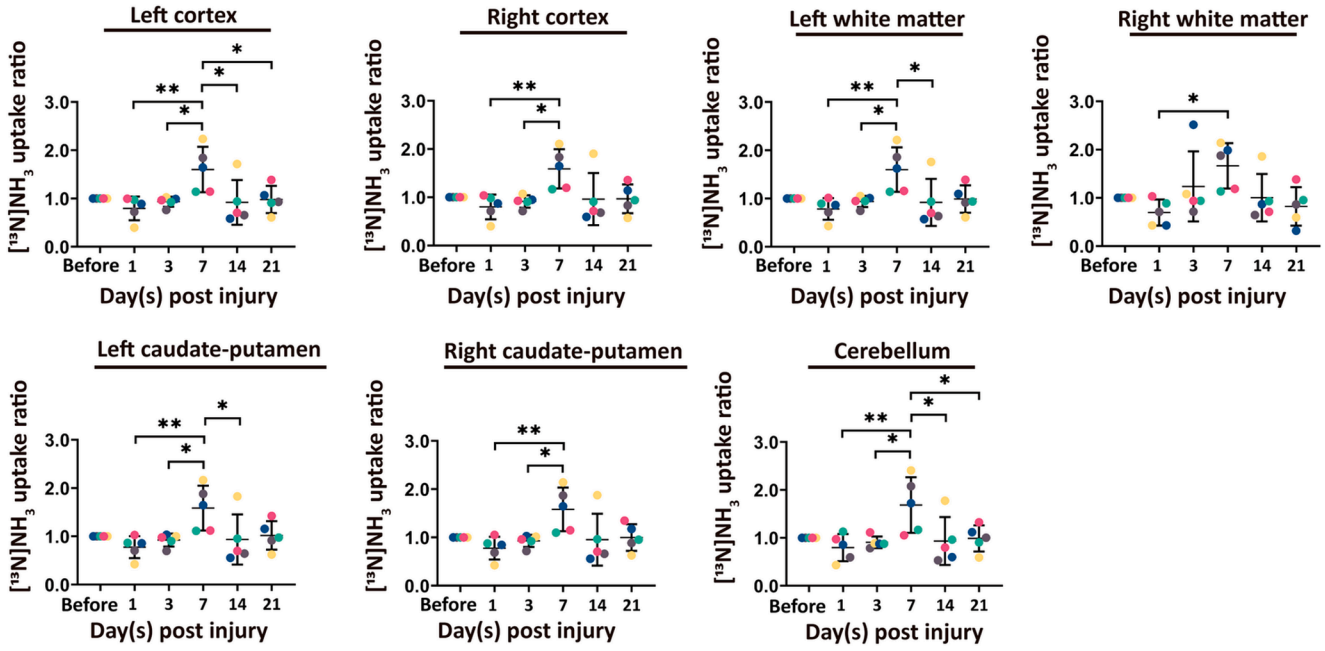

Fig. 4. [^{13}N]NH_3 uptake ratio in the cortex, white matter, caudate-putamen, and cerebellum. *p < 0.05; **p < 0.01; n = 5. Data are presented as mean ± SD. Different colors represent different dogs: grey for dog 1, yellow for dog 2, blue for dog 3, green for dog 4, and pink for dog 5. (For interpretation of the references to colour in this figure legend, the reader is referred to the web version of this article.)

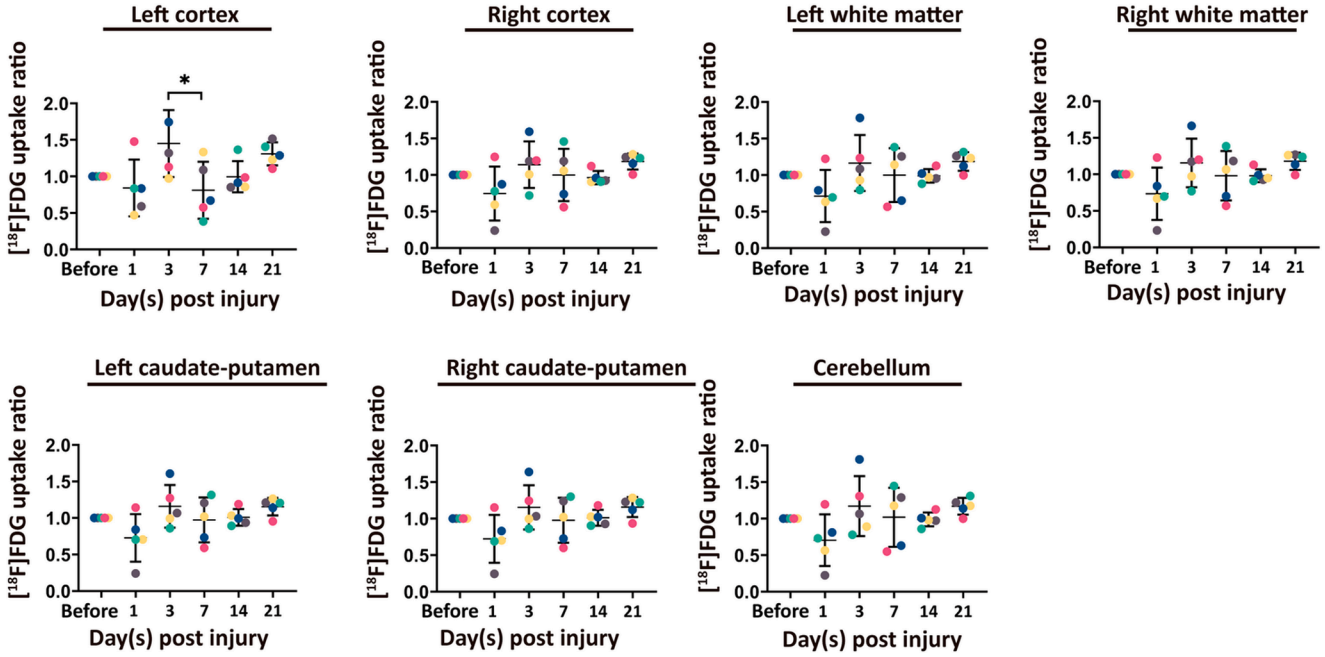

Fig. 5. [^{18}F]FDG uptake ratio in the cortex, white matter, caudate-putamen, and cerebellum. *p < 0.05; n = 5, Data are presented as mean ± SD. Different colors represent different dogs: grey for dog 1, yellow for dog 2, blue for dog 3, green for dog 4, and pink for dog 5. (For interpretation of the references to colour in this figure legend, the reader is referred to the web version of this article.)

FDG uptake in spinal cord, the uptake ratios increased and peaked at 3 days post SCI. In the left cortex, the [^{18}F]FDG uptake at 7 days post SCI decreased and was significantly lower than at 3 days post SCI (SUV_r = 1.0 ± 0.33 vs SUV_r = 1.16 ± 0.34, p = 0.036, n = 5). There was also no intergroup difference in the left-to-right ratio of [^{18}F]FDG uptake in all analyzed brain regions (p > 0.05, n = 5) (Supplementary Fig. 3). The [^{18}F]FDG uptake ratios between the analyzed regions and the whole brain were also calculated, and there was no significant intergroup difference (p > 0.05, n = 5) (Supplementary Fig. 4).

3.2. *Longitudinal [^{13}N]NH_3 and [^{18}F]FDG PET imaging in the spinal cord*

Table 1 displays the [^{13}N]NH_3 and [^{18}F]FDG uptake at the injury site (Fig. 6A). After injury, both [^{13}N]NH_3 and [^{18}F]FDG uptake increased over time. The [^{13}N]NH_3 uptake peaked at 7 days after the SCI (SUV = 1.15 ± 0.27, SUV_r = 1.55 ± 0.25). The maximum [^{18}F]FDG uptake was reached at 3 days after the SCI (SUV = 1.64 ± 0.42, SUV_r = 1.80 ± 0.55). At 14 days post SCI, the [^{13}N]NH_3 uptake began to decline over time. At

Table 1
[^{13}N]NH_3 (n = 5) and [^{18}F]FDG (n = 4) uptake in the spinal cord.

	0 day	1 day	3 days	7 days	14 days	21 days
[^{13}N]NH_3						
SUV (T9-T10)	0.55 ± 0.14	0.73 ± 0.20	0.81 ± 0.18	1.15 ± 0.27*	1.10 ± 0.55	0.8 7 ± 0.11
$SUV_{reference}$ (T4-T5)	0.62 ± 0.17	0.59 ± 0.15	0.61 ± 0.12	0.76 ± 0.19	0.69 ± 0.20	0.67 ± 0.11
SUV_r	0.88 ± 0.13	1.24 ± 0.14	1.33 ± 0.10*	1.55 ± 0.25***	1.54 ± 0.31***	1.32 ± 0.22*
[^{18}F]FDG						
SUV (T9-T11)	0.70 ± 0.09	0.98 ± 0.14	1.64 ± 0.42***	1.17 ± 0.36	0.80 ± 0.08	0.86 ± 0.17
$SUV_{reference}$ (T4-T5)	0.77 ± 0.06	0.69 ± 0.12	0.85 ± 0.21	0.81 ± 0.07	0.67 ± 0.11	0.74 ± 0.10
SUV_r	0.83 ± 0.18	1.28 ± 0.38	1.80 ± 0.55**	1.06 ± 0.39*	0.93 ± 0.31	1.00 ± 0.22

Footnotes: Data are presented as the mean ± SD. [^{18}F]FDG: 2-deoxy-2-[^{18}F] fluoroglucose; T9: the nineth thoracic segment; SUV: mean standardized uptake value at surgery site, for [^{13}N]NH_3 imaging at T9-T10 region; for [^{18}F]FDG imaging at T9-T11region; $SUV_{reference}$: mean standardized uptake value at reference region, T4-T5; SUV_r: the ratio of SUV to $SUV_{reference}$. A one-way ANOVA followed by Tukey's multiple comparisons tests was used to evaluate the difference between SUV values measured before and after the SCI. *p < 0.05; **p < 0.01; ***p < 0.001.

7 days post SCI, the [^{18}F]FDG uptake declined. There was no correlation between [^{13}N]NH_3 uptake and [^{18}F]FDG uptake (p > 0.05).

3.3. Plasma levels of MCP-1

MCP-1 is a chemokine that induces BSCB disruption (Echeverry et al., 2011). We used this biomarker to validate BSCB permeability. Plasma MCP-1 levels were measured using an ELISA kit at different time points after SCI (Fig. 6B). The baseline MCP-1 level was 154.2 ± 68.1 pg/mL before SCI. Starting from 1 day post SCI, the MCP-1 level increased over time. The MCP-1 level was highest (341.9 ± 87.1) at 7 days post injury and then decreased over time. There was a significant correlation between MCP-1 levels and the SUV and SUV_r of [^{13}N]NH_3 (p = 0.0003, r^2 = 0.3804 and p = 0.04, r^2 = 0.1412, respectively) (Fig. 6C, D).

3.4. ZO-1 expression in spinal cord

The expression of ZO-1 in the spinal cords of the control group and SCI group 21 days after injury was measured using immunostaining (Fig. 7A). The ZO-1 immunostaining intensity in the SCI group at 21 days after injury declined in comparison with the control group, but the difference was not significant (p > 0.05) (Fig. 7B).

4. Discussion

Longitudinal [^{13}N]NH_3 PET imaging revealed an increase in GS activity in all analyzed brain regions in the subacute phase of SCI compared with the acute phase. Glucose uptake after SCI was quantified using [^{18}F]FDG PET imaging in spinal cord and brain. The results of

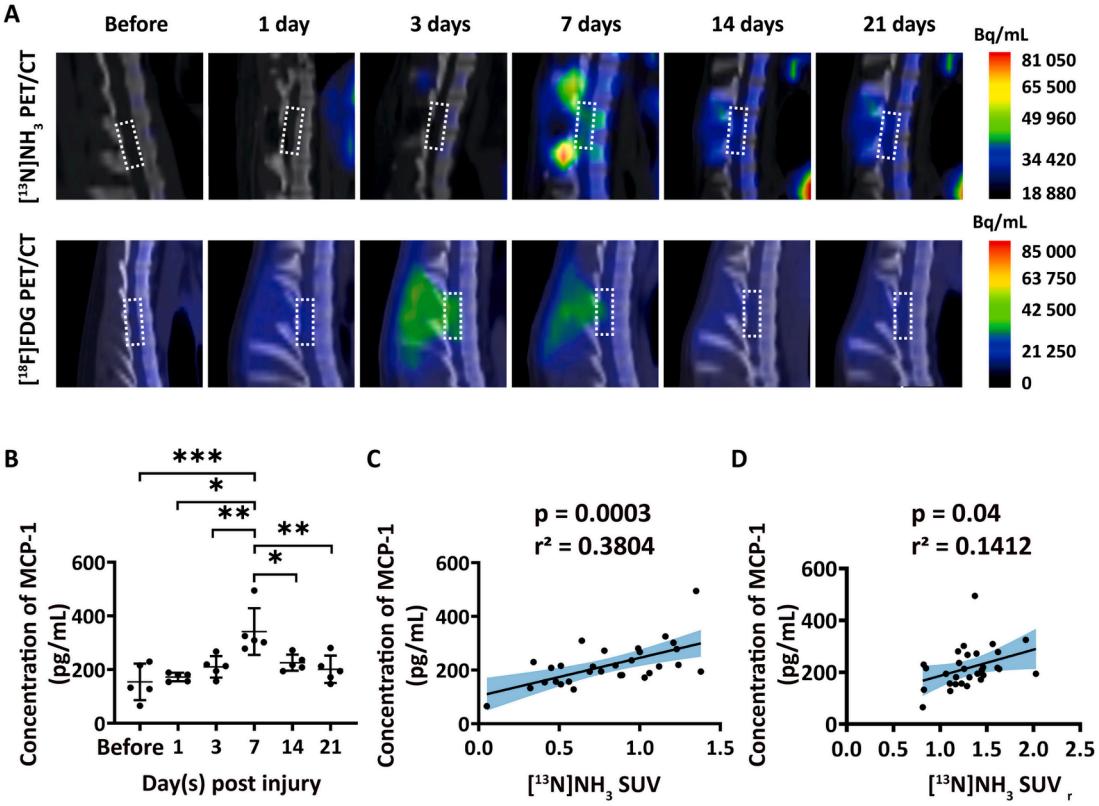

Fig. 6. [^{18}F]FDG and [^{13}N]NH_3 PET/CT studies in the spinal cord. (A) Representative longitudinal [^{13}N]NH_3 (top) and [^{18}F]FDG (bottom) PET/CT images acquired up to 21 days post SCI in the spinal cord. The [^{13}N]NH_3 uptake peaked in the spinal cord at 7 days post SCI. In contrast, the maximum [^{18}F]FDG uptake was reached at 3 days after injury. (B) The concentrations of plasma monocyte chemoattractant protein-1 (MCP-1) (n = 5 per time point, mean ± SD). The concentration of plasma MCP-1 correlated significantly with the (C) mean standardized uptake value (SUV), and (D) uptake value ratio (SUV_r) of [^{13}N]NH_3, with strong Pearson correlation coefficients. *p < 0.05; **p < 0.01; ***p < 0.001.

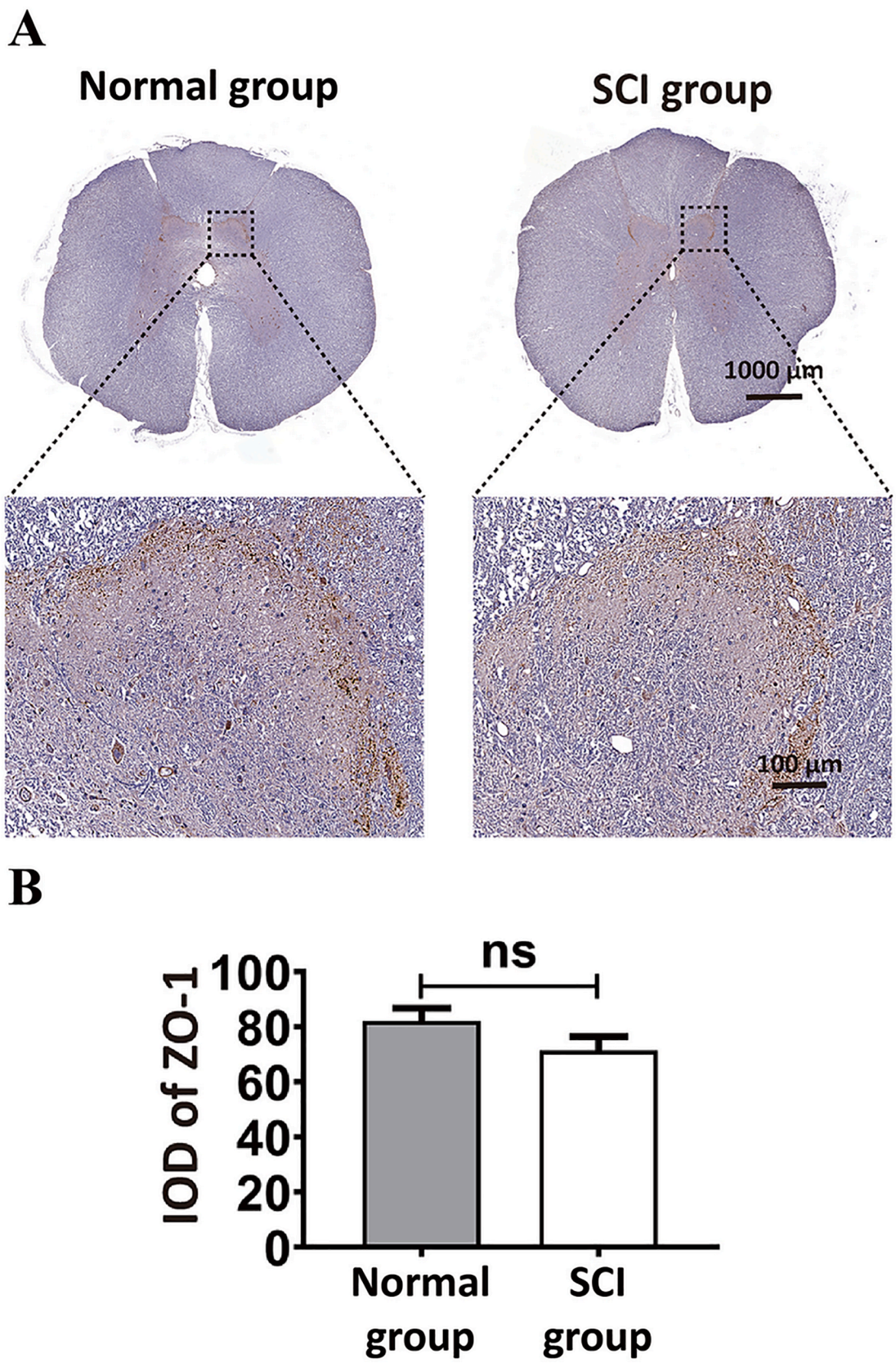

Fig. 7. Immunohistochemical assay of the penetrability of the blood-spinal cord barrier. Anti-zonula occluden 1 (ZO-1) immunostaining in the spinal cord tissue of the normal group (n = 3) and the SCI group at 21 days after injury (n = 5). (B) Average staining intensity (integrated optical density, IOD) of ZO-1 positive area. Data are presented as mean ± SD, n = 3 per group. ns, no significance.

[^{13}N]NH_3 PET imaging in the spinal cord showed the lack of [^{13}N]NH_3 penetration through the intact BSCB before SCI, and a significant correlation between the [^{13}N]NH_3 uptake and the BSCB permeability after SCI.

4.1. [^{18}F]FDG PET imaging in brain and spinal cord

The glucose analogue [^{18}F]FDG was used to quantify glucose uptake. After left-side hemisection SCI, glucose uptake increased and peaked in the spinal cord 3 days post SCI. Similar increases were seen in regions of the brain, especially the left cortex, although the difference was not significant. Our previous studies using a rat model showed that neuroinflammation in the spinal cord increases significantly during the subacute stage of SCI (Zhang et al., 2019, 2021). Other studies have shown that glycolytic pathways are upregulated and result in a large increase in [^{18}F]FDG uptake during inflammation (O'Neill and Hardie, 2013; Mochizuki et al., 2001; Vaidyanathan et al., 2015). Von Leden et al. have demonstrated that the increased [^{18}F]FDG uptake is caused by an elevated glial cell response, as histology revealed a persistent loss of neurons and increased microglia/macrophage and astrocyte activation (von Leden et al., 2016). Although it has not been clearly defined the glucose uptake regions of the brain after SCI, several studies have shown that SCI induces neuroinflammation with increased microglial activation in many brain regions, including the cortex (Wu et al., 2014a, 2014b, 2016). It is possible that the increased [^{18}F]FDG accumulation around the injury site in the spinal cord and left cortex were induced by neuroinflammation following SCI. Histological examination to assess neuronal viability and glial activity should be included in future work.

4.2. [^{13}N]NH_3 PET imaging in the brain

The uptake of [^{13}N]NH_3 showed obvious changes in all analyzed brain regions. The observed trends in GS activity in the brain after SCI are the same as those previously reported in the spinal cord. In the acute stage of SCI, GS activity in spinal cord has been reported to decline (Diaz-Ruiz et al., 2016; Liu et al., 2013), though in this study the decrease in GS activity in brain was not significant. Oxidative stress and inflammation contribute to the decrease in GS activity (Eid et al., 2013; Liu et al., 2013), which in turn restricts inflammation by inducing astrocyte migration (Zou et al., 2011). Baek et al. reported that brain is enriched in gene expression related to the oxidative phosphorylation Kyoto Encyclopedia of Gene and Genomes (KEGG) pathway in the acute phase of SCI (Baek et al., 2017). SCI-induced oxidative stress and inflammation in the brain might reduce the activity of GS.

Compared with the acute phase of SCI, in the subacute phase GS activity in the brain was increased and peaked at 7 days post SCI. Other studies have also observed an increase of GS activity in the spinal cord with a peak at 7 days post SCI (Liu et al., 2013; Benton et al., 2000). GS is a neuroprotectant and the upregulation of GS activity protects neurons from the deleterious effects of excess glutamate (Gorovits et al., 1997). Glutamine is an oxidizable energy source (Tildon and Roeder, 1984), a precursor of neurotransmitter amino acids (Albrecht et al., 2010), and a neuroprotectant against H_2O_2-induced stress (Chen and Herrup, 2012). Increased glutamine synthetase activity results in increased glutamine production in reactive astrocytes (Benton et al., 2000). Therefore, in both the spinal cord and the brain, in the subacute phase of SCI, global glutamine synthetase activity increased and produced a correspondingly high glutamine level in response to SCI.

4.3. [^{13}N]NH_3 PET imaging in spinal cord

In addition to brain, we also aimed to assess the GS activity in the spinal cord using [^{13}N]NH_3 PET. However, the PET/CT imaging showed that [^{13}N]NH_3 could not penetrate the intact BSCB before injury in contrast to the clear penetration of the blood brain barrier (BBB) for brain imaging (Supplementary Fig. 5). After injury, the uptake of [^{13}N]NH_3 into the BSCB increased over time, and peaked at 7 days post SCI. Moreover, at the 7-day time point, the reference site (T4–T5) uptake had also increased. This increased BSCB permeability at a site distant from the injury site could have occurred when the damaged cells released toxic or inflammatory substances that caused damage at other sites (Matsushita et al., 2015). Consequently, the uptake of [^{13}N]NH_3 increased at the injury site and the region distal from the injure site in the spinal cord. In the process of BSCB repair, [^{13}N]NH_3 uptake decreased over time.

In order to quantify BSCB permeability, plasma MCP-1 levels were measured. MCP-1 is a chemokine released by damaged neurons after nerve injury (Zhang and De Koninck, 2006). It is one of the major chemokines involved in CNS inflammatory processes. MCP-1 has been shown to regulate BSCB function (Echeverry et al., 2011). After openings occur in the BSCB, MCP-1 stimulates immune cell trafficking across the BSCB. In this study, plasma MCP-1 levels were significantly correlated with [^{13}N]NH_3 accumulation at the injury site. This indicates that [^{13}N]NH_3 uptake may correlate with BSCB permeability. ZO-1 is a peripheral membrane protein associated with the cytoplasmic surfaces of tight junctions (Stevenson et al., 1986; Balda and Anderson, 1993). The breakdown of BSCB results in a reduction in ZO-1 expression (Gottardi et al., 1996; Winkler et al., 2014; Henkel et al., 2009). In this study, we observed a slight decrease in the expression of ZO-1 in the spinal cord of the SCI group while the uptake of [^{13}N]NH_3 showed a slight increase. These findings together suggest that [^{13}N]NH_3 could serve as a useful PET probe for determining BSCB permeability *in vivo*. Although contributes to the secondary injury after SCI, the permeability of BSCB also provides a window for therapeutic intervention (Bartanusz et al., 2011; Sun et al., 2019). Molecules and cells with therapeutical potentials can access the central nervous system through the disrupted BSCB. Thus, monitor the permeability of BSCB *in vivo* would have implications in the therapeutic decisions for SCI patients in clinical settings.

Ammonia exists in two forms: the non-ionic form, NH_3 (~1.5% at physiological pH), and the cationic form, NH_4^+. It was long thought that NH_3 could pass freely through cell membranes and the BBB because it is a small non-ionic molecule. However, with a dipole moment of 1.47 D, which is close to that of water (1.85 D), NH_3 actually has little ability to pass through plasma membranes. Instead, it was found that the aquaporins and aquaglyceroporins in cell membranes are permeable to NH_3 (Cooper et al., 2002; Jahn et al., 2004; Zeuthen et al., 2006). For example, aquaporin-4 (AQP4) is highly expressed beyond 3 days post SCI (Nesic et al., 2006), and it contributes to SCI-induced edema (Moe et al., 2008). AQP4 has been shown to be a transmembrane channel for NH_3 (Assentoft et al., 2016). Thus, increases in aquaporin expression could be partly responsible for the [^{13}N]NH_3 uptake we observed after SCI.

Most [^{13}N]NH_3 exists as the cation, NH_4^+, which is unable to pass through plasma membranes. However, because the ionic radius of [^{13}N]NH_3 is similar to that of K^+ (152 pm), NH_4^+ is transported by K^+-selective transporters and channels (Hall et al., 1992). It has been reported that in the normal spinal cord with intact myelin there is very little outward K^+ current from axons. However, after nerve injury and demyelination, increases were detected in a persistent, outward K^+ current (Chiu and Ritchie, 1980). Another study suggested that demyelination might cause a change in K^+ channel expression in axons (Nashmi and Fehlings, 2001). However, no studies have focused on K^+ channels in the BSCB. Therefore, we hypothesize that changes in K^+ channel expression in the BSCB might play an important role in [^{13}N]NH_3 uptake in the spinal cord. Other transporters and channels, such as the rhesus-associated glycoproteins, have also been shown to transport NH_3 and NH_4^+ (Caner et al., 2015). However, no studies have investigated whether an SCI causes changes in the expression levels of these transporters and channels in the BSCB.

This study has some limitations. All five dogs in the SCI group underwent [^{13}N]NH_3 PET/CT and [^{18}F]FDG PET/CT scanning. To study inflammation after an SCI, we excluded anti-inflammatory treatments

from the study design. However, one dog had a surgical wound infection, which was treated with debridement. We therefore excluded that dog from the analysis of [^{18}F]FDG PET/CT data in spinal cord. The major limitation of using a canine model in a longitudinal study was that it was not possible to perform pathology studies or *ex vivo* studies at each time point. Nevertheless, our findings provide new avenues of research for future projects. Another limitation might be the low resolution of human PET/CT for canine model scanning and the partial volume effect. There might be some spill-out signal in spinal cord imaging. However, it is clear from the [^{13}N]NH_3 PET/CT imaging in the spinal cord that the high signal in the surrounding tissues does not cause significant spill-out signal in the spinal cord. Also, the accumulation of the tracer in the surrounding tissue was very low where there was high uptake in the spinal cord tissue. Therefore, we presume that the spill-out signal in the spinal cord is insignificant. Because of the limited human PET/CT resolution, there might be possibility that the [^{13}N]NH_3 uptake in spinal cord was underestimated before SCI. Future studies should investigate histological changes and the correlations with *ex vivo* markers to determine the accuracy of the findings in this study. Moreover, it would be very interesting to explore the mechanism underlying our findings. On the other hand, a clinical trial might be the optimal method for determining whether [^{13}N]NH_3 PET/CT will be useful in detecting human BSCB permeability in future clinical applications.

5. Conclusion

In this longitudinal study, we evaluated the uptake of [^{18}F]FDG and [^{13}N]NH_3 in the spinal cord and brain before and after SCI in a canine hemisection SCI model to assess the influence of SCI on cerebral energy and glutamate metabolism *in vivo*. We found an increase in glucose uptake in the spinal cord after SCI and a similar increase that was not statistically significant in the brain. GS activity in the brain was also higher in the subacute phase of SCI than in the acute phase. [^{13}N]NH_3 uptake in the spinal cord correlated with BSCB permeability; this provides an *in vivo* imaging method of assessing BSCB permeability that could be suitable for use in a clinical setting.

6. Data and code availability statement

The de-identified datasets and corresponding code used in this study are available from the corresponding author upon reasonable request.

Funding

This work was supported by the Key Research Projects of the Ningxia Hui Autonomous Region [Grant No. 2018BCG01002] and the Natural Science Fund of Ningxia Hui Autonomous Region [Grant No. 2018AAC02012].

CRediT authorship contribution statement

Lijian Zhang: Investigation, Methodology, Data curation, Formal analysis. **Francisco R. López-Picón:** Methodology, Formal analysis, Writing - review & editing. **Yingqin Jia:** Investigation. **Yao Chen:** Investigation. **Juan Li:** Resources. **Chunlei Han:** Resources, Software. **Xiaoqing Zhuang:** Conceptualization, Investigation, Formal analysis, Writing - original draft, Writing - review & editing. **Hechun Xia:** Conceptualization, Supervision, Funding acquisition.

Declaration of Competing Interest

The authors declare that they have no known competing financial interests or personal relationships that could have appeared to influence the work reported in this paper.

Acknowledgements

The authors gratefully acknowledge Prof. Merja Haaparanta-Solin from the Turku PET Centre for support and assistance, and Dr. Wenchang Xiao and Dr. Lu Wan from Huazhong University of Science & Technology for their work in MRI scanning of the dogs.

Appendix A. Supplementary data

Supplementary data to this article can be found online at https://doi.org/10.1016/j.nicl.2021.102692.

References

Athanasiou, A., Klados, M.A., Pandria, N., et al., 2017. A systematic review of investigations into functional brain connectivity following spinal cord injury. Front. Hum. Neurosci. 11, 517. https://doi.org/10.3389/fnhum.2017.00517.

Assentoft, M., Kaptan, S., Schneider, H.P., Deitmer, J.W., de Groot, B.L., MacAulay, N., 2016. Aquaporin 4 as a NH3 channel. J. Biol. Chem. 291 (36), 19184–19195. https://doi.org/10.1074/jbc.M116.740217.

Albrecht, J., Sidoryk-Węgrzynowicz, M., Zielińska, M., Aschner, M., 2010. Roles of glutamine in neurotransmission. Neuron. Glia. Biol. 6 (4), 263–276. https://doi.org/10.1017/S1740925X11000093.

Baek, A., Cho, S.R., Kim, S.H., 2017. Elucidation of gene expression patterns in the brain after spinal cord injury. Cell Transplant. 26 (7), 1286–1300. https://doi.org/10.1177/0963689717715822.

Balda, M.S., Anderson, J.M., 1993. Two classes of tight junctions are revealed by ZO-1 isoforms. Am. J. Physiol. 264 (4 Pt 1), C918–C924. https://doi.org/10.1152/ajpcell.1993.264.4.C918.

Bartanusz, V., Jezova, D., Alajajian, B., Digicaylioglu, M., 2011. The blood-spinal cord barrier: morphology and clinical implications. Ann. Neurol. 70 (2), 194–206. https://doi.org/10.1002/ana.22421.

Benton, R.L., Ross, C.D., Miller, K.E., 2000. Glutamine synthetase activities in spinal white and gray matter 7 days following spinal cord injury in rats. Neurosci. Lett. 291 (1), 1–4. https://doi.org/10.1016/s0304-3940(00)01362-8.

Bock, P., Spitzbarth, I., Haist, V., et al., 2013. Spatio-temporal development of axonopathy in canine intervertebral disc disease as a translational large animal model for nonexperimental spinal cord injury. Brain Pathol. 23 (1), 82–99. https://doi.org/10.1111/j.1750-3639.2012.00617.x.

Caner, T., Abdulnour-Nakhoul, S., Brown, K., Islam, M.T., Hamm, L.L., Nakhoul, N.L., 2015. Mechanisms of ammonia and ammonium transport by rhesus-associated glycoproteins. Am. J. Physiol. Cell Physiol. 309 (11), C747–C758. https://doi.org/10.1152/ajpcell.00085.2015.

Choi, D.W., Rothman, S.M., 1990. The role of glutamate neurotoxicity in hypoxic-ischemic neuronal death. Annu. Rev. Neurosci. 13, 171–182. https://doi.org/10.1146/annurev.ne.13.030190.001131.

Cooper, A.J., McDonald, J.M., Gelbard, A.S., Gledhill, R.F., Duffy, T.E., 1979. The metabolic fate of 13N-labeled ammonia in rat brain. J. Biol. Chem. 254 (12), 4982–4992.

Cooper, G.J., Zhou, Y., Bouyer, P., Gritchenko, I.I., Boron, W.F., 2002. Transport of volatile solutes through AQP1. J. Physiol. 542 (Pt 1), 17–29. https://doi.org/10.1113/jphysiol.2002.023218.

Cooper, A.J., Plum, F., 1987. Biochemistry and physiology of brain ammonia. Physiol. Rev. 67 (2), 440–519. https://doi.org/10.1152/physrev.1987.67.2.440.

Chiu, S.Y., Ritchie, J.M., 1980. Potassium channels in nodal and internodal axonal membrane of mammalian myelinated fibres. Nature 284 (5752), 170–171. https://doi.org/10.1038/284170a0.

Chen, J., Herrup, K., 2012. Glutamine acts as a neuroprotectant against DNA damage, beta-amyloid and H2O2-induced stress. PLoS One 7 (3), e33177. https://doi.org/10.1371/journal.pone.0033177.

Diaz-Ruiz, A., Montes, S., Salgado-Ceballos, H., Maldonado, V., Rivera-Espinosa, L., Ríos, C., 2016. Enzyme activities involved in the glutamate-glutamine cycle are altered to reduce glutamate after spinal cord injury in rats. NeuroReport 27 (18), 1317–1322. https://doi.org/10.1097/WNR.0000000000000700.

Echeverry, S., Shi, X.Q., Rivest, S., Zhang, J., 2011. Peripheral nerve injury alters blood-spinal cord barrier functional and molecular integrity through a selective inflammatory pathway. J. Neurosci. 31 (30), 10819–10828. https://doi.org/10.1523/JNEUROSCI.1642-11.2011.

Eid, T., Tu, N., Lee, T.S., Lai, J.C., 2013. Regulation of astrocyte glutamine synthetase in epilepsy. Neurochem. Int. 63 (7), 670–681. https://doi.org/10.1016/j.neuint.2013.06.008.

Freund, P., Weiskopf, N., Ward, N.S., et al., 2011. Disability, atrophy and cortical reorganization following spinal cord injury. Brain 134 (Pt 6), 1610–1622. https://doi.org/10.1093/brain/awr093.

Gorovits, R., Avidan, N., Avisar, N., Shaked, I., Vardimon, L., 1997. Glutamine synthetase protects against neuronal degeneration in injured retinal tissue. Proc. Natl. Acad. Sci. USA 94 (13), 7024–7029. https://doi.org/10.1073/pnas.94.13.7024.

Gottardi, C.J., Arpin, M., Fanning, A.S., Louvard, D., 1996. The junction-associated protein, zonula occludens-1, localizes to the nucleus before the maturation and during the remodeling of cell-cell contacts. Proc. Natl. Acad. Sci. USA 93 (20), 10779–10784. https://doi.org/10.1073/pnas.93.20.10779.

Hall, M.C., Koch, M.O., McDougal, W.S., 1992. Mechanism of ammonium transport by intestinal segments following urinary diversion: evidence for ionized NH4+ transport via K(+)-pathways. J. Urol. 148 (2 Pt 1), 453–457. https://doi.org/10.1016/s0022-5347(17)36627-2.

Hains, B.C., Saab, C.Y., Waxman, S.G., 2005. Changes in electrophysiological properties and sodium channel Nav1.3 expression in thalamic neurons after spinal cord injury. Brain 128 (Pt 10), 2359–2371. https://doi.org/10.1093/brain/awh623.

Henkel, J.S., Beers, D.R., Wen, S., Bowser, R., Appel, S.H., 2009. Decreased mRNA expression of tight junction proteins in lumbar spinal cords of patients with ALS. Neurology 72 (18), 1614–1616. https://doi.org/10.1212/WNL.0b013e3181a41228.

Jahn, T.P., Møller, A.L., Zeuthen, T., Holm, L.M., Klaerke, D.A., Mohsin, B., Kühlbrandt, W., Schjoerring, J.K., 2004. Aquaporin homologues in plants and mammals transport ammonia. FEBS. Lett. 574 (1–3), 31–36. https://doi.org/10.1016/j.febslet.2004.08.004.

Liu, C., Wu, W., Zhang, B., Xiang, J., Zou, J., 2013. Temporospatial expression and cellular localization of glutamine synthetase following traumatic spinal cord injury in adult rats. Mol. Med. Rep. 7 (5), 1431–1436. https://doi.org/10.3892/mmr.2013.1383.

Matsushita, T., Lankford, K.L., Arroyo, E.J., Sasaki, M., Neyazi, M., Radtke, C., Kocsis, J. D., 2015. Diffuse and persistent blood-spinal cord barrier disruption after contusive spinal cord injury rapidly recovers following intravenous infusion of bone marrow mesenchymal stem cells. Exp. Neurol. 267, 152–164. https://doi.org/10.1016/j.expneurol.2015.03.001.

Mergenthaler, P., Lindauer, U., Dienel, G.A., Meisel, A., 2013. Sugar for the brain: the role of glucose in physiological and pathological brain function. Trends. Neurosci. 36 (10), 587–597. https://doi.org/10.1016/j.tins.2013.07.001.

Moe, S.E., Sorbo, J.G., Sogaard, R., Zeuthen, T., Petter Ottersen, O., Holen, T., 2008. New isoforms of rat Aquaporin-4. Genomics 91 (4), 367–377. https://doi.org/10.1016/j.ygeno.2007.12.003.

Mohammed, H., Hollis, E.R., 2nd., 2018. Cortical reorganization of sensorimotor systems and the role of intracortical circuits after spinal cord injury. Neurotherapeutics. 15 (3), 588–603. https://doi.org/10.1007/s13311-018-0638-z.

Mochizuki, T., Tsukamoto, E., Kuge, Y., et al., 2001. FDG uptake and glucose transporter subtype expressions in experimental tumor and inflammation models. J. Nucl. Med. 42 (10), 1551–1555.

Momosaki, S., Ito, M., Tonomura, M., Abe, K., 2015. Assessment of glutamine synthetase activity by [13N]ammonia uptake in living rat brain. Synapse 69 (1), 26–32. https://doi.org/10.1002/syn.21781.

Moore, S.A., Granger, N., Olby, N.J., et al., 2017. Targeting translational successes through CANSORT-SCI: using pet dogs to identify effective treatments for spinal cord injury. J. Neurotrauma. 34 (12), 2007–2018. https://doi.org/10.1089/neu.2016.4745.

Nashmi, R., Fehlings, M.G., 2001. Mechanisms of axonal dysfunction after spinal cord injury: with an emphasis on the role of voltage-gated potassium channels. Brain Res. Brain Res. Rev. 38 (1–2), 165–191. https://doi.org/10.1016/s0165-0173(01)00134-5.

Nesic, O., Lee, J., Ye, Z., Unabia, G.C., Rafati, D., Hulsebosch, C.E., Perez-Polo, J.R., 2006. Acute and chronic changes in aquaporin 4 expression after spinal cord injury. Neuroscience 143 (3), 779–792. https://doi.org/10.1016/j.neuroscience.2006.08.079.

O'Neill, L.A., Hardie, D.G., 2013. Metabolism of inflammation limited by AMPK and pseudo-starvation. Nature 493 (7432), 346e55. https://doi.org/10.1038/nature11862.

Rothman, S.M., Olney, J.W., 1986. Glutamate and the pathophysiology of hypoxic–ischemic brain damage. Ann. Neurol. 19 (2), 105–111. https://doi.org/10.1002/ana.410190202.

Roelcke, U., Curt, A., Otte, A., et al., 1997. Influence of spinal cord injury on cerebral sensorimotor systems: a PET study. J. Neurol. Neurosurg. Psychiatr. 62 (1), 61–65. https://doi.org/10.1136/jnnp.62.1.61.

Ryu, H.H., Lim, J.H., Byeon, Y.E., et al., 2009. Functional recovery and neural differentiation after transplantation of allogenic adipose-derived stem cells in a canine model of acute spinal cord injury. J. Vet. Sci. 10 (4), 273–284. https://doi.org/10.4142/jvs.2009.10.4.273.

Solstrand Dahlberg, L., Becerra, L., Borsook, D., Linnman, C., 2018. Brain changes after spinal cord injury, a quantitative meta-analysis and review. Neurosci. Biobehav. Rev. 90, 272–293. https://doi.org/10.1016/j.neubiorev.2018.04.018.

Stevenson, B.R., Siliciano, J.D., Mooseker, M.S., Goodenough, D.A., 1986. Identification of ZO-1: a high molecular weight polypeptide associated with the tight junction (zonula occludens) in a variety of epithelia. J. Cell Biol. 103 (3), 755–766. https://doi.org/10.1083/jcb.103.3.755.

Sun, G., Zeng, S., Liu, X., et al., 2019. Synthesis and characterization of a silica-based drug delivery system for spinal cord injury therapy. Nano-Micro Lett. 11, 23. https://doi.org/10.1007/s40820-019-0252-6.

Tildon, J.T., Roeder, L.M., 1984. Glutamine oxidation by dissociated cells and homogenates of rat brain: kinetics and inhibitor studies. J. Neurochem. 42 (4), 1069–1076. https://doi.org/10.1111/j.1471-4159.1984.tb12712.x.

Winkler, E.A., Sengillo, J.D., Sagare, A.P., Zhao, Z., Ma, Q., Zuniga, E., Wang, Y., Zhong, Z., Sullivan, J.S., Griffin, J.H., Cleveland, D.W., Zlokovic, B.V., 2014. Blood-spinal cord barrier disruption contributes to early motor-neuron degeneration in ALS-model mice. Proc. Natl. Acad. Sci. USA 111 (11), E1035–E1042. https://doi.org/10.1073/pnas.1401595111.

Wrigley, P.J., Gustin, S.M., Macey, P.M., et al., 2009. Anatomical changes in human motor cortex and motor pathways following complete thoracic spinal cord injury. Cereb Cortex 19 (1), 224–232. https://doi.org/10.1093/cercor/bhn072.

Wu, J., Zhao, Z., Sabirzhanov, B., et al., 2014a. Spinal cord injury causes brain inflammation associated with cognitive and affective changes: role of cell cycle pathways. J. Neurosci. 34 (33), 10989–11006. https://doi.org/10.1523/JNEUROSCI.5110-13.2014.

Wu, J., Stoica, B.A., Luo, T., et al., 2014b. Isolated spinal cord contusion in rats induces chronic brain neuroinflammation, neurodegeneration, and cognitive impairment. Involvement of cell cycle activation. Cell Cycle 13 (15), 2446–2458. https://doi.org/10.4161/cc.29420.

Wu, J., Zhao, Z., Kumar, A., et al., 2016. Endoplasmic reticulum stress and disrupted neurogenesis in the brain are associated with cognitive impairment and depressive-like behavior after spinal cord injury. J. Neurotrauma. 33 (21), 1919–1935. https://doi.org/10.1089/neu.2015.4348.

Vaidyanathan, S., Patel, C.N., Scarsbrook, A.F., Chowdhury, F.U., 2015. FDG PET/CT in infection and inflammation-current and emerging clinical applications. Clin. Radiol. 70 (7), 787–800. https://doi.org/10.1016/j.crad.2015.03.010.

von Leden, R.E., Selwyn, R.G., Jaiswal, S., Wilson, C.M., Khayrullina, G., Byrnes, K.R., 2016. (18)F-FDG-PET imaging of rat spinal cord demonstrates altered glucose uptake acutely after contusion injury. Neurosci. Lett. 621, 126–132. https://doi.org/10.1016/j.neulet.2016.04.027.

Yoon, E.J., Kim, Y.K., Shin, H.I., Lee, Y., Kim, S.E., 2013. Cortical and white matter alterations in patients with neuropathic pain after spinal cord injury. Brain Res. 1540, 64–73. https://doi.org/10.1016/j.brainres.2013.10.007.

Yoon, E.J., Kim, Y.K., Kim, H.R., Kim, S.E., Lee, Y., Shin, H.I., 2014. Transcranial direct current stimulation to lessen neuropathic pain after spinal cord injury: a mechanistic PET study. Neurorehabil. Neural. Repair. 28 (3), 250–259. https://doi.org/10.1177/1545968313507632.

Zalkin, H., Smith, J.L., 1998. Enzymes utilizing glutamine as an amide donor. Adv. Enzymol. Relat. Areas. Mol. Biol. 72, 87–144. https://doi.org/10.1002/9780470123188.ch4.

Zeuthen, T., Wu, B., Pavlovic-Djuranovic, S., Holm, L.M., Uzcategui, N.L., Duszenko, M., Kun, J.F., Schultz, J.E., Beitz, E., 2006. Ammonia permeability of the aquaglyceroporins from Plasmaodium falciparum, Toxoplasmaa gondii, and Trypanosoma brucei. Mol. Microbiol. 61 (6), 1598–1608. https://doi.org/10.1111/j.1365-2958.2006.05325.x.

Zhang, L., Zhuang, X., Chen, Y., Niu, Z., Xia, H., 2020. Plasma erythropoietin, IL-17A, and IFNγ as potential biomarkers of motor function recovery in a canine model of spinal cord injury. J. Mol. Neurosci. 70 (11), 1821–1828. https://doi.org/10.1007/s12031-020-01575-y.

Zhang, L., Zhuang, X., Chen, Y., Xia, H., 2019. Intravenous transplantation of olfactory bulb ensheathing cells for a spinal cord hemisection injury rat model. Cell Transplant. 28 (12), 1585–1602. https://doi.org/10.1177/0963689719883842.

Zhang, L., Zhuang, X., Kotitalo, P., et al., 2021. Intravenous transplantation of olfactory ensheathing cells reduces neuroinflammation after spinal cord injury via interleukin-1 receptor antagonist. Theranostics 11 (3), 1147–1161. https://doi.org/10.7150/thno.52197.

Zhang, J., De Koninck, Y., 2006. Spatial and temporal relationship between monocyte chemoattractant protein-1 expression and spinal glial activation following peripheral nerve injury. J. Neurochem. 97 (3), 772–783. https://doi.org/10.1111/j.1471-4159.2006.03746.x.

Zou, J., Wang, Y.X., Mu, H.J., et al., 2011. Down-regulation of glutamine synthetase enhances migration of rat astrocytes after in vitro injury. Neurochem Int. 58 (3), 404–413. https://doi.org/10.1016/j.neuint.2010.12.018.